Received: 28 February 2020 | Revised: 12 May 2020 | Accepted: 30 May 2020

DOI: 10.1111/ejn.14853

SPECIAL ISSUE ARTICLE

EJN European Journal of Neuroscience FENS WILEY

Fine structure analysis of perineuronal nets in the ketamine model of schizophrenia

Rahul Kaushik[1,2]* | **Nikita Lipachev**[1,3]* | **Gabriela Matuszko**[1] | **Anastasia Kochneva**[4] | **Anastasia Dvoeglazova**[4] | **Axel Becker**[5] | **Mikhail Paveliev**[6,7] | **Alexander Dityatev**[1,2,8]

[1]Molecular Neuroplasticity, German Center for Neurodegenerative Diseases (DZNE), Magdeburg, Germany

[2]Center for Behavioral Brain Sciences (CBBS), Magdeburg, Germany

[3]Institute of Physics, Kazan Federal University, Kazan, Russia

[4]Institute of Fundamental Medicine and Biology, Kazan Federal University, Kazan, Russia

[5]Institute of Pharmacology and Toxicology, Faculty of Medicine, Otto-von-Guericke-University Magdeburg, Magdeburg, Germany

[6]Danish Research Institute of Translational Neuroscience, Aarhus University, Aarhus, Denmark

[7]Neuroscience Center, University of Helsinki, Helsinki, Finland

[8]Medical Faculty, Otto-von-Guericke University, Magdeburg, Germany

Correspondence
Alexander Dityatev, German Center for Neurodegenerative Diseases (DZNE), Leipziger Str. 44, Haus 64, Magdeburg 39120, Germany.
Email: alexander.dityatev@dzne.de

Funding
N.L. was supported by a short-term fellowship from German Academic Exchange Service DAAD and an honorary scholarship from the Russian government. A.K. was supported by an honorary scholarship from Kazan Federal University. The work was supported by the Russian Government Program of Competitive Growth of Kazan Federal University, and by the Bundesministerium für Bildung und Forschung (BMBF) to A.D (EnergI project 01GQ1421A).

Abstract

Perineuronal nets (PNNs) represent a highly condensed specialized form of brain extracellular matrix (ECM) enwrapping mostly parvalbumin-positive interneurons in the brain in a mesh-like fashion. PNNs not only regulate the onset and completion of the critical period during postnatal brain development, control cell excitability, and synaptic transmission but are also implicated in several brain disorders including schizophrenia. Holes in the perineuronal nets, harboring the synaptic contacts, along with hole-surrounding ECM barrier can be viewed as PNN compartmentalization units that might determine the properties of synapses and heterosynaptic communication. In this study, we developed a novel open-source script for Fiji (ImageJ) to semi-automatically quantify structural alterations of PNNs such as the number of PNN units, area, mean intensity of PNN marker expression in 2D and 3D, shape parameters of PNN units in the ketamine-treated Sprague–Dawley rat model of schizophrenia using high-resolution confocal microscopic images. We discovered that the mean intensity of ECM within PNN units is inversely correlated with the area and the perimeter of the PNN holes. The intensity, size, and shape of PNN units proved to be three major principal factors to describe their variability. Ketamine-treated rats

Abbreviations: CSPGs, Chondroitin sulfate proteoglycans; ECM, Brain extracellular matrix; GAGs, Glycosaminoglycans; KS test, Kolmogorov–Smirnov; NMDARs, N-methyl-D-aspartate receptors; PFC, Prefrontal cortex; PNN, Perineuronal nets; PV, Parvalbumin; WFA, Wisteria floribunda agglutinin.
*Shared first authors.

Edited by Prof. Constanze Seidenbecher

The peer review history for this article is available at https://publons.com/publon/10.1111/ejn.14853

had more numerous but smaller and less circular PNN units than control rats. These parameters allowed to correctly classify individual PNNs as derived from control or ketamine-treated groups with ≈85% reliability. Thus, the proposed multidimensional analysis of PNN units provided a robust and comprehensive morphometric fingerprinting of fine ECM structure abnormalities in the experimental model of schizophrenia.

KEYWORDS

chondroitin sulfate proteoglycans, extracellular matrix, parvalbumin, Wisteria floribunda agglutinin, synapses

1 | INTRODUCTION

Schizophrenia is a devastating neuropsychiatric disorder characterized by both positive and negative symptoms, rendering patients to social as well as occupational dysfunction (Bitanihirwe, Mauney, & Woo, 2016; Mueser & McGurk, 2004). Dysregulations of dopaminergic as well as glutamatergic neurotransmitter systems have been widely implicated in the pathogenesis of schizophrenia (Gomes & Grace, 2018; Grace, 2016; Moghaddam & Javitt, 2012). Hyperdopaminergia in striatal regions and hypodopaminergia in the prefrontal cortical regions suggest a complex dysregulation of dopaminergic system (Abi-Dargham & Moore, 2003; Lau, Wang, Hsu, & Liu, 2013; Mitelman et al., 2019; Slifstein et al., 2015). More recently, the glutamate neurotransmitter system has also been implicated in the pathogenesis of schizophrenia as glutamatergic dysfunction can explain both positive and negative symptoms, (Banerjee, Zuck, Yablonsky-Alter, & Lidsky, 1995; Carlsson, 1995; Heresco-Levy, 2005; Olney & Farber, 1995) as well as cognitive dysfunctions such as social recognition (Le Gall & Iakimova, 2018), prospective memory (Wang, Chan, & Shum, 2018), and hot executive functions (MacKenzie et al., 2017). Several molecular and genetic insights along with the fact that ketamine-mediated inhibition of N-methyl-D-aspartate receptors (NMDARs) transiently induce symptoms of acute schizophrenia led to the hypothesis of glutamatergic dysfunction in the origin of schizophrenia (Morris, Cochran, & Pratt, 2005; Stefanovic et al., 2009; Stone et al., 2008). Ketamine (2-chlorphenyl-2-methylamino-cyclohexanone) is a non-competitive antagonist of NMDAR that binds to a phencyclidine-binding site within the ion pore of the channel. Although ketamine is primarily a ligand for NMDAR, it also has varying degree of affinities for several other receptors, most notably for the high-affinity state of the D2 dopamine receptor and serotonin 5-HT2A receptors (Frohlich & Van Horn, 2014; Hunt, Kessal, & Garcia, 2005; Kapur & Seeman, 2002; Vernaleken et al., 2013). The non-NMDAR receptor affinities of ketamine are confounding factors for the glutamate hypothesis of schizophrenia but make ketamine an excellent drug that has the potential to unify these competing hypotheses into a single, multi-transmitter hypothesis that might underlie the pathogenesis of schizophrenia.

Pathological changes in schizophrenia are marked by decreased GABAergic signaling, an altered ratio of excitation/inhibition and changes in gamma oscillations, affecting several brain regions including the prefrontal cortex (PFC) (Castillo-Gomez, Perez-Rando, Vidueira, & Nacher, 2016; Castillo-Gomez, Varea, Blasco-Ibanez, Crespo, & Nacher, 2016; Chung, Fish, & Lewis, 2016; Matuszko, Curreli, Kaushik, Becker, & Dityatev, 2017; McNally, McCarley, & Brown, 2013; Sohal, 2014; Steullet et al., 2018). Parvalbumin-expressing (PV+) fast-spiking GABAergic interneurons provide inhibitory control of cortical and subcortical circuits and seem to be highly relevant to the pathophysiology of schizophrenia. The density of PV+ interneurons in the mice models of schizophrenia as well as human post mortem PFC was intensively examined in the context of the disease for the past decade. The outcome of these studies is contradictory as some studies found a reduced density of PV+ interneurons (Beasley & Reynolds, 1997; Bitanihirwe & Woo, 2014a; Reynolds, Beasley, & Zhang, 2002; Sakai et al., 2008), while other reported no changes in the density of PV+ interneurons (Alcaide et al., 2019; Chung et al., 2016; Enwright et al., 2016; Hashimoto et al., 2003; Tooney & Chahl, 2004; Woo, Miller, & Lewis, 1997). However, a recent meta-analysis study confirmed the reduction of parvalbumin-expressing interneurons in the PFC of schizophrenic patients (Kaar, Angelescu, Marques, & Howes, 2019).

Recent studies also point to schizophrenia-associated changes in the perineuronal nets (PNNs) associated with PV+ neurons in brain areas such as PFC. PNNs are lattice-like 3 dimensional (3D) structures that are mostly associated with PV+ interneurons covering the somata, proximal segments of dendrites, and the axonal initial segment. PNNs are formed by proteoglycans carrying complex sugars called glycosaminoglycans (GAGs) assembled with a backbone of hyaluronic acid, link proteins, and tenascin-R

(Dityatev & Schachner, 2003; Dityatev, Schachner, & Sonderegger, 2010). PNNs can be labeled with a commonly used lectin named *Wisteria floribunda* agglutinin (WFA) that binds to N-acetyl-galactosamine residues within chondroitin sulfate chains (Arnst et al., 2016; Kaushik et al., 2018). PNNs are widely expressed in several regions of the brain such as cortex, hippocampus, cerebellum, and the spinal cord (Dityatev, Wehrle-Haller, & Pitkanen, 2014; Ferrer-Ferrer & Dityatev, 2018). Several studies have shown the physiological importance of PNN in stabilizing the synaptic contacts and regulating cell excitability, excitatory input to PV+ cells, synaptic plasticity, protection from oxidative stress, receptor mobility, cell surface distribution of neurotrophic factors, cation binding sites, and glutamate spillover (Bernard & Prochiantz, 2016; Carulli et al., 2010; Celio, Spreafico, De Biasi, & Vitellaro-Zuccarello, 1998; Dityatev et al., 2007; Dityatev, Frischknecht, & Seidenbecher, 2006; Hayani, Song, & Dityatev, 2018; Heine et al., 2008; Kochlamazashvili et al., 2010; Lander, Zhang, & Hockfield, 1998; McRae, Rocco, Kelly, Brumberg, & Matthews, 2007; Miyata & Kitagawa, 2015; Morawski, Bruckner, Riederer, Bruckner, & Arendt, 2004; Pizzorusso et al., 2002; Sorg et al., 2016). Moreover, structural alterations in PNNs have been strongly implicated in several pathological conditions such as Alzheimer's disease, stroke, epilepsy, depression, autism, and schizophrenia (Berezin, Walmod, Filippov, & Dityatev, 2014; Dityatev & Fellin, 2008; Kwok, Dick, Wang, & Fawcett, 2011; Lodge, Behrens, & Grace, 2009; Miyata & Kitagawa, 2015; Morawski, Filippov, Tzinia, Tsilibary, & Vargova, 2014; Riga et al., 2017; Soleman, Filippov, Dityatev, & Fawcett, 2013). We have previously reported a reduction in the density of WFA+ cells in the PFC of ketamine-treated rats as a model of schizophrenia (Matuszko et al., 2017). A similar tendency was observed for PV+ WFA+cells, with no changes were detected in the density of PV+ and PV+ WFA- cells.

Holes in the net-like structure of PNN are occupied by the synaptic boutons largely originating from other interneurons, but also from excitatory cells, suggesting the important role of PNNs in shaping the perisomatic innervation of PV+ cells (Arnst et al., 2016; Dityatev et al., 2007; Lipachev et al., 2019; Sigal, Bae, Bogart, Hensch, & Zhuang, 2019). A hole together with the surrounding perisynaptic ECM barrier can be viewed as a structural and functional PNN unit. Considering the arrangement of synaptic boutons within such unit, it can be well conceived that amount of ECM proteins assembled within an individual unit, GAGs expression on these ECM proteins and their geometric arrangement might critically affect the properties of synaptic transmission and hence neuronal communication (Eill, Sinha, Morawski, Viapiano, & Matthews, 2020; Hayani et al., 2018). Despite both the physiological and pathological importance of the PNNs, the PNN units have received far less attention, presumably due to a lack of a proper tool for quantitative analysis of these PNN fine structures. In this study, we acquired high-resolution confocal images of PNNs from the PFC of wild-type control as well as ketamine-treated rats as a model of schizophrenia. We developed an algorithm to semi-automatically measure parameters related to the fine organization of PNN units, which reflect the spatial pattern of chondroitin sulfate proteoglycans (CSPGs) distribution in PNNs. Finally, we quantified how these parameters are affected in the ketamine model of schizophrenia and discussed possible applications of the proposed approach.

2 | METHODS

2.1 | Animals

All animal experiments were conducted in accordance with ethical animal research standards defined by German law and recommendations of the Ethical Committee on Animal Health and Care of the State of Saxony-Anhalt, Germany. Eight-week-old Sprague–Dawley (MolTac: *SD*, Taconic Denmark, SPD) male rats were used in all ketamine-induced schizophrenia model experiments, as previously described (Matuszko et al., 2017). The animals were kept in controlled laboratory conditions: at 20 ± 2°C, air humidity 55%–60% and 12-hr day/night cycle (lights on at 6 a.m.). The rats were housed in a group of five animals in Macrolon IV cages until the end of ketamine treatment, with free access to food pellets (Altronim 1326) and tap water.

2.2 | Ketamine treatment

The animals were treated according to the previously published protocol (Becker et al., 2009). A timeline of the experiment is provided in Figure 1a. In brief, twelve animals received either ketamine (30 mg/kg b.w., ketamine hydrochloride, Astrapin, Pfaffen-Schwabenhein, Germany) or the vehicle (0.9% NaCl) for control. Injections were given in two sessions of 5 days, with daily injections separated by a two-day break between sessions. Injections were made intraperitoneally (IP) at a volume of 1 ml/100 g of animal weight.

Two days after the final injection, the animals were housed singly for 12 days. For the social interaction test, two days were needed as described by MacKenzie et al. (2017). Briefly, animals were familiarized to an open-field arena in two trials of 7 min each two days before the social interaction test. The day before testing, rats were allocated to test partners based on pretreatment and body weight. The difference between the two partners was within 20 g. During the test, animal pairs were placed in the arena for 7 min. Two days after completion of the behavioral experiments, the animals were sacrificed for further processing. The period between

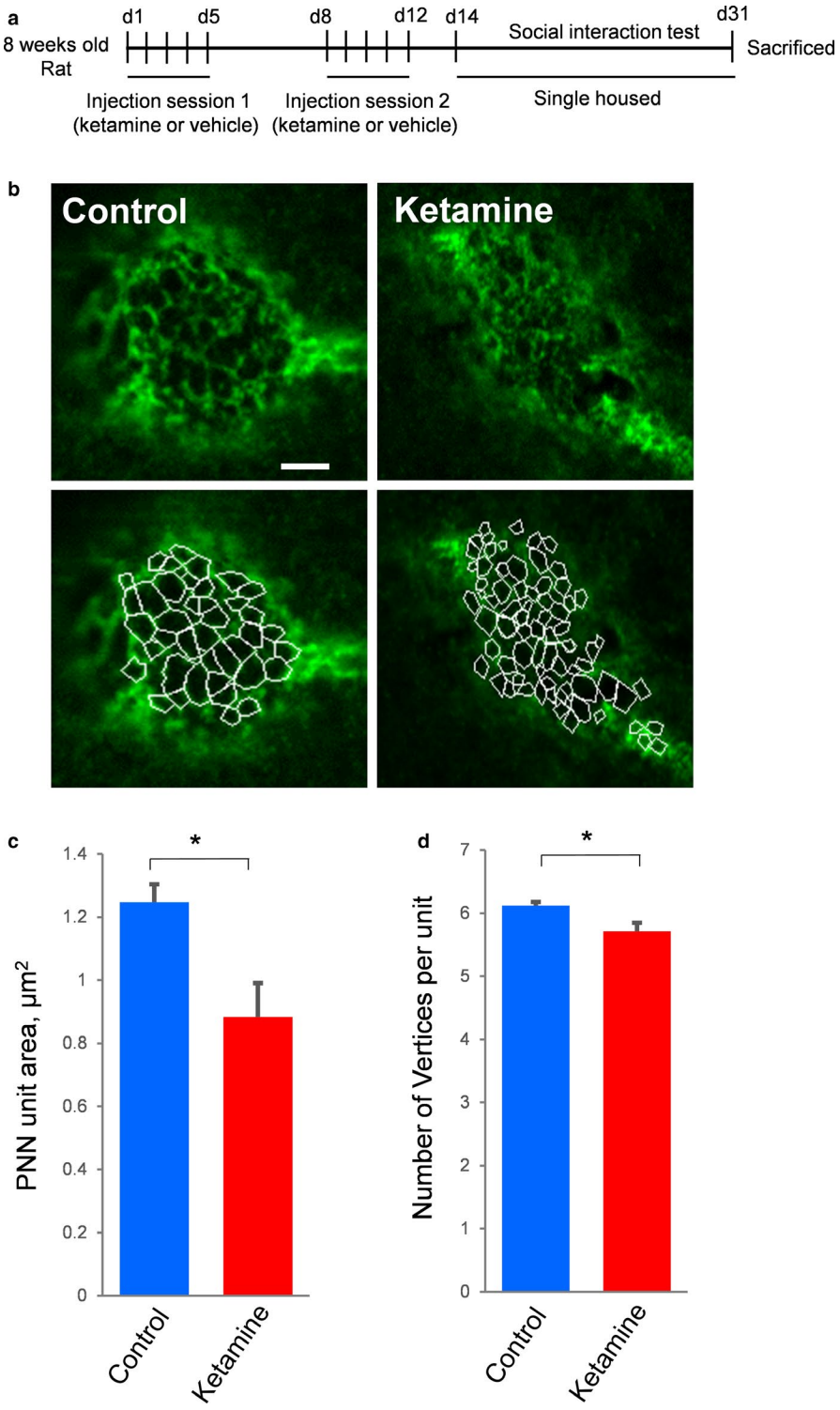

FIGURE 1 Ketamine treatment reduces the area and the number of vertices of PNN units. (a) Timeline of the experiment. (b) Representative traces of PNN units from control and ketamine-treated animals. (c-d) Quantification of unit area and the number of vertices was done in 17 cells from 4 animals for the control group and in 12 cells from 4 animals for the ketamine group. Scale bar is 3 µm

the final ketamine injection and brain collection was 18 days. This period excludes that all changes observed are due to acute substance effects.

2.3 | Immunohistochemistry

Two days after the social interaction test, animals were deeply anesthetized (400 mg/kg b.w. chloral hydrate injection) and perfused transcardially with 4% PFA. Brains were incubated overnight in 4% PFA PBS solution at +4°C, cryoprotected in 30% sucrose PB solution for 48 hr at +4°C. Then, brains were frozen in 100% 2-methyl butane at −80ºC and sliced in 50-µm-thick coronal sections. Floating sections were kept in a solution consisting of 1 part ethylene glycol, 1 part of glycerin, 2 parts of PBS, with pH = 7.2. For each staining condition, three sections per brain area of each animal were selected. All sections were washed in 120 mM phosphate

buffer (PB), pH = 7.2. For double PV and WFA staining, the medial PFC was permeabilized with PB containing 0.5% Triton X-100 (Sigma T9284) for 10 min at RT, followed by application of blocking solution (PB supplemented with 0.1% Triton X-100 and 5% normal goat serum (Gibco 16210-064) for 1 hr at RT. Afterward, sections were incubated for 48 hr in the presence of primary reagents: biotinylated Wisteria floribunda agglutinin (WFA, 1:500, Sigma, Cat no. L1516) and rabbit anti-PV antibody (whole serum SWANT PV 25 1:300 36 hr, + 4°C). Sections were washed three times in PB followed by overnight incubation at 4°C with secondary reagents, streptavidin-Alexa 488 conjugate (Thermo Fisher Scientific, Cat no. S11223, 1:1,000, 12 hr, RT), and goat anti-rabbit Alexa 546-conjugated secondary antibodies (Thermo Fisher Scientific, Cat no. A11035, 1:1,000, 3 hr, RT). Sections were washed in PB and stained for 1 hr with Hoechst 3,342 (1 mg/ml in DMSO, 1:500, Sigma B2261) and mounted on SuperFrost glasses with Fluoromount (Sigma F4680).

2.4 | Acquisition and image processing

Images of PV-immunopositive PNNs were acquired using Zeiss LSM 700 confocal microscope and EC Plan-Neofluar 20×/0.50 M27, or Plan-Apochromat 63×/1.40 oil M27 objective for PNN fine-structure analysis, while the experimenter was blinded to the treatment group. For each animal, three 50-μm-thick brain sections sampled with 200-μm distance were selected for counting. For the PNN fine-structure analysis, 8–10 images of PV+ WFA+ cells per animals were acquired in the deep layers IV and V of the prelimbic cortex as z-stacks (16-bit, 14 optical sections, 0.170 μm intervals between sections, 1,024 × 1,024 pixels, the pixel size of 0.099 μm).

2.5 | Analysis of PNN units

2.5.1 | Manual tracing of PNN units

Quantitative image analysis of single confocal planes was performed in Fiji (Schindelin et al., 2012) using a Meshes script described previously (Arnst et al., 2016). PNN units on neuronal cell bodies and proximal dendrites were traced. The PNN unit area was calculated using a Fiji script as follows: To define the unit vertices, the Fiji Point Picker tool was used. Pixels belonging to a particular unit were selected as a polygon based on the vertex coordinates and quantified using getHistogram Fiji command. The area of the unit was calculated as the sum of pixels counts for the whole range of intensity values. To investigate the distribution of fluorescence intensity along the perimeter of single units, the polarity index was calculated. Units characterized by prominent WFA signal values at vertices and lower intensity at the middles of the edges were defined as polar. On the contrary, units with the homogeneously distributed intensity of WFA were defined as nonpolar. The polarity index was calculated as the mean intensity in vertices defined by three pixels per vertex divided by the mean intensity of edge middle area defined as three pixels in the middle of the edge. It indicates WFA signal enrichment at the vertices of the unit. Then, the mean value was calculated for each neuron, for each animal, and finally – mean value for 4 animals in each experimental group.

2.5.2 | Semi-automatic tracing of PNN units

To measure the properties of PNN units, we developed a script that we named as *Analysis of Perineuronal Net Units* (APNU v1.1). The program prompts the user to choose a centrally located pixel within a hole and then the program provides an automatic outline of the PNN hole and surrounding ECM barrier. After a central point in a PNN hole is manually selected, the program computes profiles of ECM intensity along with the given number of tracking directions (20 sectors in this study) for a given number of confocal layers (3 in this study) in which a PNN unit is expected to be located. The holes are defined as areas where the ECM intensity remains lower than the mean intensity at the hole center + the given threshold. The ECM barrier coordinates are defined by local maxima in ECM intensity in a plane where the central point is located (2D ECM) or by 3D coordinates corresponding to the maximal intensities for each of tracking directions (3D ECM). If no local maximum is detected for a particular direction, linear extrapolation is used to calculate the coordinates of the ECM barrier from the coordinates of well-defined neighboring ECM barrier points. If there are too many directions for which the local maxima cannot be found (>50%), the unit is considered as not well defined and excluded from the analysis. The triangulation method was used to calculate the areas of holes and ECM barriers in 3D.

Several input parameters are used to control the measurements. Scale (X, Y, Z) defines the spatial resolution of images in XY and Z plane; Layers are the number of Z planes to be selected for the 3D analysis of the PNN units; Sectors are the number of sectors generated to dissect the 360° space around the chosen central pixel; Radius is the number of pixels taken into consideration to find the local maxima of ECM intensity (i.e., the border of ECM barrier), Manual threshold is the end user-defined threshold to separate signal from noise; Threshold percentage for skipping a layer is the percentage or ill-defined local maxima required to skip a layer from analysis; Spike to smooth and threshold percentage to smooth spikes are internal technical parameters for noisy images; Confirmation of results allows to skip objects (PNN units) that user judges to be not correctly outlined; Save 2D

polygon data allows to save the measurements of all outlines in relevant layers. The self-explanatory parameters for the illustrations of the results allow further modification of the output of the program as per the needs of the end user.

The resulting output text file contains several parameters defined as follows: IntMean2Dhole, IntMean3Dhole, IntMean2DECM, IntMean3DECM are the mean intensities of the hole and ECM in 2D and 3D space, respectively. Similarly, Area2Dhole, Area3Dhole, Area2DECM, Area3DECM are the areas of the hole and ECM in 2D and 3D space; Per2Dhole, Per3Dhole, Per2DECM, Per3DECM are the perimeters of the hole and ECM in 2D and 3D space; Circ2Dhole, AR2Dhole, Round2Dhole, Solidity2Dhole, Circ2DECM, AR2DECM, Round2DECM, Solidity2DECM are the Fiji shape parameters for holes and ECM; IntMin3DECM is the minimum intensity of ECM in 3D space to estimate the leakiness of PNN units; zSDECM is the standard deviation of ECM intensity in Z planes to estimate how flat a PNN unit is. IntMean2DECM1 is the mean intensity value of the ECM for 20 local maxima found on the lines to make sectors. IntMean2DECM2 is the mean intensity value of the ECM along the perimeter connecting the 20 local maxima. To describe how much the ECM barrier is above the level of ECM in holes, we calculated additional parameters: IntMean2DECM1corr and IntMean2DECM2corr, as differences between IntMean2DECM1 or 2 and IntMean2Dhole, and IntMean3DECMcorr and IntMean-Min_3DECM as differences between IntMean3DECM and IntMean3Dhole or IntMin3DECM, respectively.

2.6 | Statistical analysis

Statistical analysis was performed using GraphPad Prism 5.0 (GraphPad Software Inc., La Jolla, USA), Sigmaplot 13.0 (StatSoft, USA), and XLSTAT software (Addinsoft Inc, N.Y., USA). All data are shown as the mean ± *SEM*. Students' *t*-test was used to compare the means of parameters after manual tracing. We performed Spearman correlation analysis to detect the correlation between measured parameters, the Kolmogorov–Smirnov test was used to compare cumulative probability frequency distributions. The principal factor analysis with varimax rotation was performed to reveal the most informative parameters to describe the variability of PNN units. The linear discriminant and logistic regression analyses with a stepwise forward selection of most informative parameters were performed to reveal a minimal set of parameters for classification of PNNs as derived from control versus ketamine-treated animals, and the reliability of classification.

3 | RESULTS

To investigate how the properties of PNN units are affected by the ketamine treatment, we first manually analyzed and quantified the area of units and the mean number of the unit vertices.

3.1 | Ketamine treatment reduces the PNN unit area and the average number of the unit vertices

We measured the quantitative parameters of the PNN unit geometry in control and ketamine-treated animals using the previously described method (Arnst et al., 2016). We observed that the mean area of PNN unit was significantly reduced after the treatment with ketamine (0.88 ± 0.11 μm^2) as compared to control (1.24 ± 0.05 μm^2, $p = .024$; Figure 1b, c). Additionally, the mean number of ECM-enriched vertices was reduced in the units of ketamine-treated animals (5.7 ± 0.13) as compared to controls (6.11 ± 0.06, $p = .032$; Figure 1b, c). We did not observe any differences either in the distribution of the mean ECM staining intensity along the unit perimeter or the standard deviation of the intensity between the control and ketamine-treated experimental groups (data not shown).

3.2 | Measurement of PNN unit parameters using automatic tracing

The results obtained by manual tracing method encouraged us to further search for a more objective way to measure PNN units not only in 2D but also in 3D space. To this end, we developed a novel algorithm that allowed us to reliably measure several parameters related to the area, intensity, and shape of the PNN units, as illustrated in Figure 2a-d and described in the Methods. As measurements are fast, we were able to quickly analyze 5,495 PNN units/64 cells from 5 control rats

FIGURE 2 Automatic method of PNN unit quantification. (a) Representative images of PNNs associated with parvalbumin-positive interneurons in control and ketamine-treated animals. (b) Zoomed image of the yellow rectangular area from panel A, showing the reconstructions of holes and perisynaptic ECM traced by the program in 3 planes (Z − 1, Z0, Z + 1). The blue dot is the central pixel selected by the user as the center of the PNN units, the red dots in the tracings are positions of global maxima per specific direction in three z planes, cyan color pixels are the first pixels above the threshold used for the determination of holes. (c) The line profile of WFA intensity along the yellow line. The dotted red line denotes the threshold that was set to define holes. (d) Example images of PNNs and all PNN units that were traced by the program. Scale bars: 10 μm (A), 1 μm (b and c), and 5 μm (d)

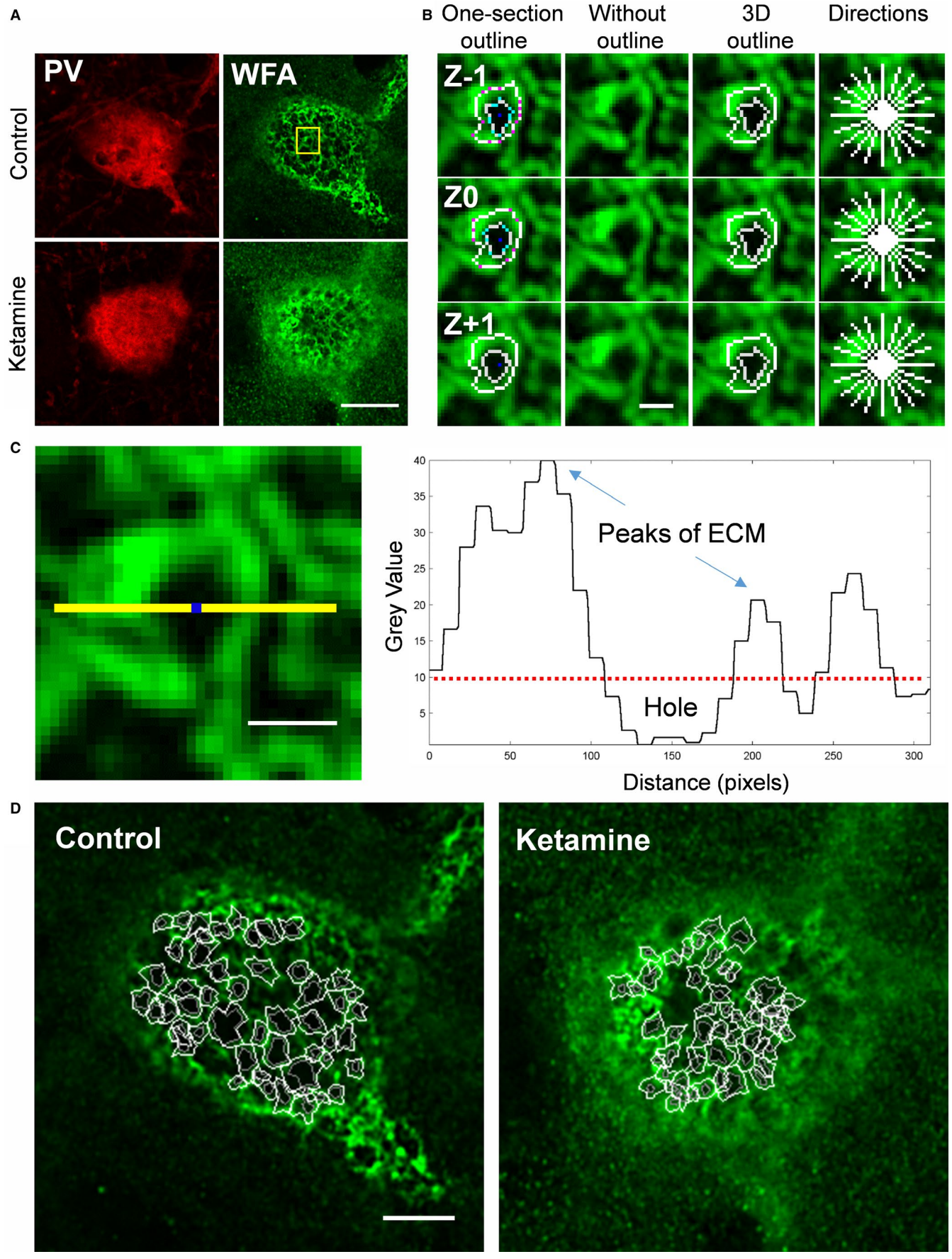
A
PV
WFA
Control
Ketamine
B
One-section outline
Without outline
3D outline
Directions
Z-1
Z0
Z+1
C
Grey Value
Peaks of ECM
Hole
Distance (pixels)
0
50
100
150
200
250
300
5
10
15
20
25
30
35
40
D
Control
Ketamine

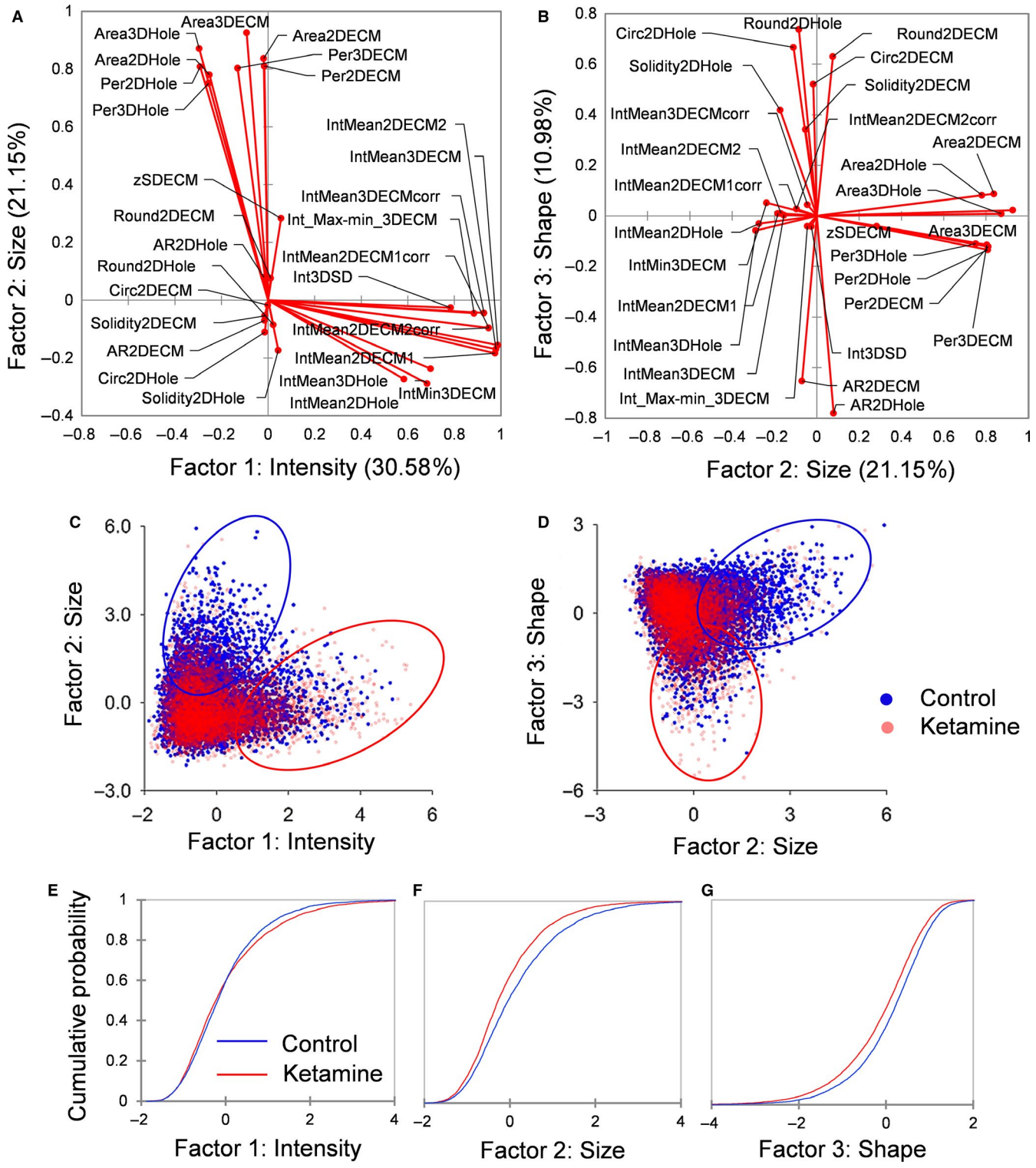

FIGURE 3 Comparison of PNN units in the representation space of the first three principal factors. (a-b) Principal factor analysis with varimax rotation revealed the intensity, size, and shape of holes/perisynaptic ECM as the three most informative factors with loads of 30.58%, 21.15%, and 10.98%, respectively. Representation of all PNN units in intensity-size and size–shape projections shows a strong overlap between two groups but also highlights clusters of PNN units distinct between control and ketamine-treated groups (outlined by ellipsoids in c-d). (e-g) Differences in cumulative frequency distributions of principal factors between control and ketamine-treated group

and 7,365 PNN units/64 cells from 6 ketamine-treated animals. The analysis was constrained to perisomatic PNN units of PV-immunopositive cells.

Firstly, we measured the correlations between all the measured parameters. This analysis revealed reasonably high correlations between 2D and 3D measures as well as some

interesting other correlations (Figure S1a-f). For instance, we observed a strong correlation between the perimeter and the area of holes in 2D space with a Spearman coefficient of correlation $\rho = 0.977$ ($p < .0001$), as well as between area of holes within individual PNN units measured in 2D and 3D space ($\rho = 0.827$, $p < .0001$). We also observed a very strong correlation between the intensities of ECM in 2D and 3D space ($\rho = 0.954$, $p < .0001$). These observations are expected and hence suggest the reliability of the method. More interestingly, we observed a moderate but highly significant negative correlation between the mean intensity of ECM and either perimeter ($\rho = -0.474$, $p < .0001$) or area of PNN holes ($\rho = -0.493$, $p < .0001$).

3.3 | Principal factor analysis revealed the intensity, the size, and the shape of holes/perisynaptic ECM as major factors determining the variability of PNN units

To better understand the interdependencies between our PNN measures, we performed a principal factor analysis that allows constructing the linear combinations of closely interrelated measures (factors) that would maximally explain the variability of PNN units and to perform the varimax rotation of these factors to facilitate the interpretation of the results. Our analysis revealed intensity, size, and the shape of holes/perisynaptic ECM as the three most informative factors with loads of ≈31%, 21%, and 11% of the total variance, respectively (Figure 3a, b). Representation of all PNN units in the intensity-size and size-shape projections shows a strong overlap between control and ketamine groups but also highlights regions of parameter values where the groups are distinct (Figure 3c, d). Additionally, the plots of cumulative distributions of PNN unit factor values indicate a smaller size and different shape of the ketamine-treated group as compared to control (Figure 3e-g).

3.4 | Multiple parameters of PNN units are significantly altered after ketamine treatment

A comparison of cumulative distribution functions of individual PNN unit parameters in control and ketamine-treated rats using the Kolmogorov–Smirnov (KS) test revealed significant differences in all parameters with p-values well below 0.05 (Figure S2A). The most prominent changes were observed in IntMean2DECM2 ($p < .0001$), IntMean3DECM ($p < .0001$), Area3DHole ($p < .0001$), Area3DECM ($p < .0001$), Circ2DHole ($p < .0001$), Circ2DECM ($p < .0001$), Area2DHole ($p < .0001$), Area2DECM ($p < .0001$), which and are plotted individually in Figure S2A-I.

The KS test revealed significant differences in the distributions of various PNN parameters also after averaging PNN unit values per cell (Figure 4a). The notable individual distributions are plotted to highlight the alterations after ketamine treatment (Figure 4c-f). Interestingly, the ECM area was significantly smaller in the ketamine group as compared to controls, which is in line with the results of the manual analysis of a smaller fraction of cells.

Furthermore, we performed the two-sample *t*-test for various parameters after averaging cell values per animal (Figure 4b). Multiple differences between control and ketamine-treated rats were detected in key parameters such as the number of PNN units (86.7 ± 3.35 versus 112.3 ± 7.6, $p = .019$), circularity (0.670 ± 0.006 versus 0.647 ± 0.001, $p = .024$) and solidity of 2D ECM (0.876 ± 0.003 versus 0.866 ± 0.001, $p = .011$; Figure 4g-j). Also the area of 3D ECM had a tendency to be smaller in the ketamine group (0.876 ± 0.008 versus 0.866 ± 0.003, $p = .09$; Figure 4j).

3.5 | Reliable discrimination of control and treated cells based on PNN parameters

To reveal the minimal set of parameters (mean PNN unit values per cell) for discrimination of cells from control and ketamine-treated rats, we performed the linear discriminant analysis with a stepwise forward selection of most informative parameters. This analysis revealed that parameters related to the circularity and solidity of ECM in 2D space together with the number of PNN units are the key parameters to discriminate between two groups (Figure 5a, b). Importantly, the linear classifier allowed correct identification of 83.59% of cells from the control group and ketamine groups (Figure 5c). The receiver operating characteristic (ROC) curve illustrates the diagnostic ability of the linear classifier, describing the relationship between its specificity and sensitivity (Figure 5d).

To further investigate if we can improve the cell classification using another approach, we performed the logistic regression analysis with a stepwise forward selection of PNN parameters. Again, the circularity of ECM in 2D and the number of PNN units turned out to be the most informative parameters to discriminate between PNNs from control and ketamine-treated rats. The classifier provided correct discrimination of PNNs from the control group and ketamine group for 85.16% of cells (Figure S3A-C).

3.6 | Correlation between parameters of PNN units and the size and the intensity of the PV + cells

Previous studies have revealed a loss of PV+ cells and/or reduction in PV expression in schizophrenia patients and

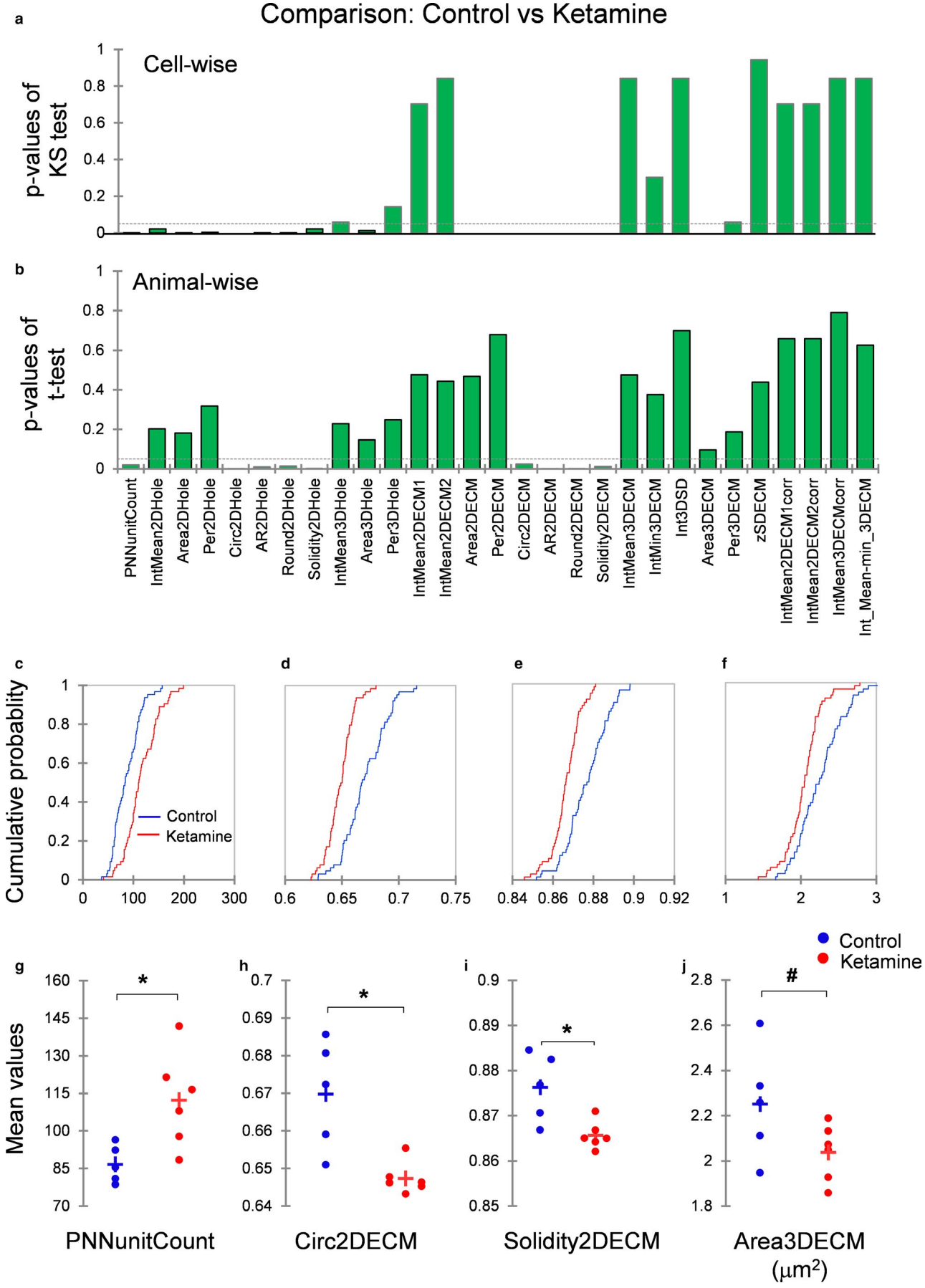
a
Comparison: Control vs Ketamine
Cell-wise
p-values of KS test
b
Animal-wise
p-values of t-test
PNNunitCount
IntMean2DHole
Area2DHole
Per2DHole
Circ2DHole
AR2DHole
Round2DHole
Solidity2DHole
IntMean3DHole
Area3DHole
Per3DHole
IntMean2DECM1
IntMean2DECM2
Area2DECM
Per2DECM
Circ2DECM
AR2DECM
Round2DECM
Solidity2DECM
IntMean3DECM
IntMin3DECM
Int3DSD
Area3DECM
Per3DECM
zSDECM
IntMean2DECM1corr
IntMean2DECM2corr
IntMean3DECMcorr
Int_Mean-min_3DECM
c
d
e
f
Cumulative probablity
Control
Ketamine
g
h
i
j
Control
Ketamine
Mean values
PNNunitCount
Circ2DECM
Solidity2DECM
Area3DECM
(μm²)

animal models (Bitanihirwe & Woo, 2014b; Jeevakumar et al., 2015; Kaar et al., 2019). Importantly, changes in the expression of PV have been tightly linked to the structural maturation of PNNs (Sigal et al., 2019). Hence, we investigated if the levels of PV expression may correlate with parameters of fine PNN structure (Figure S4A-D). We also considered the size (area) of PV+ cells as this parameter reflects the variability of PV+ cell subtypes. The size reliably correlated with PV intensity in control ($\rho = 0.416$, p-value = .001) and ketamine-treated rats ($\rho = 0.259$, $p = .039$). In both groups, there was a correlation between PV expression and number of PNN units (control: $\rho = 0.354$, $p = .004$; ketamine: $\rho = 0.34$, $p = .006$). Only in the ketamine group, there were significant correlations between the size of PV+ cells and the intensity of ECM in holes ($\rho = -0.271$, $p = .03$), circularity ($\rho = 0.308$, $p = .013$) and solidity ($\rho = 0.380$, $p = .002$) of PNN units, but not with any other parameters. Thus, three parameters that were revealed to be the most informative for discrimination between control and ketamine groups by the linear discriminant analysis, proved to depend either on the PV intensity or size of PV+ cells in the ketamine-treated rats.

4 | DISCUSSION

In the present study, we have identified some key structural alterations in the PNN units after ketamine treatment using a novel open-source script for Fiji (ImageJ). We observed that area, perimeter, intensity, and shape measurements of PNN units in 2D and 3D space can be valuable quantifiable properties that can be reliably used to investigate the structural alterations of these PNN substructures in pathological conditions. Using manual tracing, we observed a decreased mean PNN unit area and the number of vertices after treatment with ketamine, suggesting morphological alterations. Interestingly, using our semi-automatic method, we also observed a decrease in the circularity index after ketamine treatment that is in line with the lower number of vertices observed with manual tracing. Moreover, analysis of individual PNNs revealed a smaller 3D area of PNN units after ketamine treatment as observed with manual tracing.

Furthermore, we discovered that the mean intensity of WFA around holes of PNN significantly and inversely correlates with the area of the hole. Moreover, we also observed a strong positive correlation between the 2D and 3D measurements of area and mean intensity of WFA. The discriminant analysis revealed the circularity and solidity of ECM and the number of PNN units as major parameters to discriminate between control and ketamine treated PNNs. Strikingly the precision of PNN discrimination by linear discriminant analysis or by logistic regression analysis was about 85%, that is, similar to the precision of discrimination between healthy people and schizophrenia patients on the basis on the most established biomarker of schizophrenia such as prepulse inhibition (Yang et al., 2017). Collectively, we conclude that multidimensional analysis of PNN units can be a robust and comprehensive tool to detect abnormalities in the fine structures of PNN units.

Transmission electron microscopy studies have suggested that PNNs might physically inhibit the pre- and postsynaptic terminals (Bruckner, Kacza, & Grosche, 2004). Several fluorescence microscopy studies along with super-resolution STED microscopy data also support the idea that PNN may represent physical barriers between synapses (Geissler et al., 2013; Miyata, Komatsu, Yoshimura, Taya, & Kitagawa, 2012), which may affect spillover of molecules released from a synapse to the neighboring ones and regulate heterosynaptic plasticity. Interestingly, we observed that smaller holes might have a proportionally higher ECM and vice versa, suggesting a relationship exists between individual synapses and the surrounding extracellular matrix. It is plausible that bigger PNN holes might represent the large ECM-free space on the surface of soma, which remains to be innervated. Vice versa, high WFA levels may correspond to PNN units surrounding active synapses that might release ECM molecules to aggregate and fill perisynaptic space, reducing the size of holes. Alternatively, some set of active synapses may release ECM-degrading proteases that will increase the PNN hole area and reduce the intensity of ECM.

Despite increasing interest and research on the structure and function of PNNs, there are several open PNN-related questions. How do ECM molecules assemble around the synapses leading to the development of mature PNNs? How various shapes and sizes of PNN holes correlate with the properties of synaptic boutons? How the structural changes within individual PNN units affect the stability of the synaptic connections and regulate the synaptic plasticity? How the presence of GAGs and their sulfation might contribute to fine organization of PNNs? How heterogeneity among the population of PV+ cells and their afferent projections correlate with the properties of individual PNN units? Answers to these questions heavily rely on the existence and quality of a tool that can be used to reliably quantify different properties of PNN units.

FIGURE 4 The number of PNN units, circularity and solidity of 2D ECM, and the area of 3D ECM are significantly altered after ketamine treatment. (a) Bar graph representing the p-values of the KS test for cumulative frequency distributions of all parameters related to PNN units averaged per cell after ketamine treatment. (b) Bar graph representing the p-values for the effect of ketamine treatment on mean values of PNNs averaged per animal calculated using the Student's t-test. (c-f) Cumulative distribution functions for significantly different parameters. (g-j) Dots represent mean values of parameters per animal in control and ketamine-treated rats, + shows the mean of means. $^{*}p < .05$, $^{\#}p < .1$

A Stepwise forward discriminant analysis for cells:

Parameter	*F*	Pr > *F*
Circularity of ECM in 2D	60.530	< 0.0001
PNN unit count	31.490	< 0.0001
Solidity of ECM in 2D	5.455	0.021

B

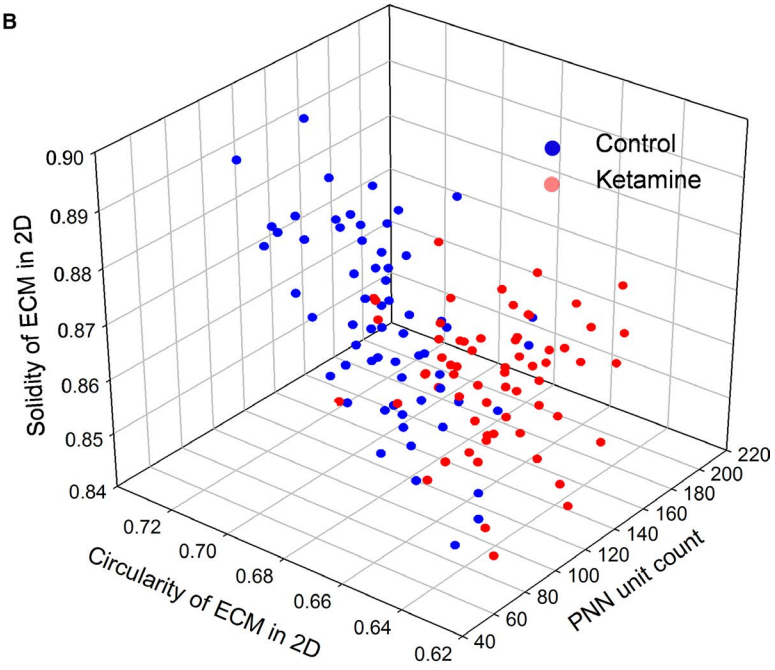

C Confusion matrix for the cross-validation results:

from \ to	Control	Ketamine	Total	% correct
Control	54	10	64	84.38%
Ketamine	11	53	64	82.81%
Total	65	63	128	83.59%

D

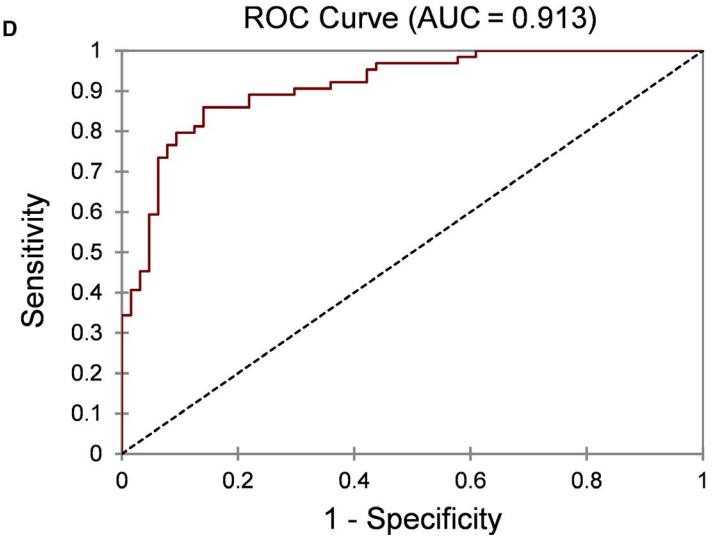

FIGURE 5 The discriminant analysis of PNNs with a stepwise forward selection of informative parameters. (a) The number of PNN units, the circularity and solidity of ECM in 2D turned out to be the most informative parameters to discriminate between PNNs from control and ketamine-treated rats. (b) Cell representation in the space of three most informative for group discrimination parameters shows an excellent separation between ketamine and control groups. (c) The classifier allows the 83.59% correct prediction of PNN units from both the control and ketamine groups. (d) The ROC curve describing the relationship between the specificity and sensitivity of the classifier. AUC, the area under the ROC curve

It has been reported that PNNs can be very heterogeneous (Arnst et al., 2016) and their properties have critically been linked to the maturation of PV+ interneurons (Begum & Sng, 2017; Racz, Gaal, & Matesz, 2016). The accumulation of PNNs around PV+ cells acts as a molecular brake on synaptic plasticity and marks the closing of critical periods of plasticity (Sigal et al., 2019). Moreover, the increase in the expression of parvalbumin has been directly linked to increased activity of parvalbumin cells that might result into activity-dependent accumulation of PNN and hence marks the maturation of inhibitory cortical circuitry (Carceller, Guirado, & Nacher, 2019; Dityatev et al., 2007; Favuzzi et al., 2017; Patz, Grabert, Gorba, Wirth, & Wahle, 2004). Interestingly, we also observed a moderate but significant positive correlation of the number of PNN units, circularity and solidity of ECM in 2D with either intensity or the size of PV + cells after the treatment with ketamine, suggesting the treatment induces modification in PNNs depending on the level of PV+ cell activity and subtype.

As per a recently published study, the structural maturation of PNN seems to follow a stereotypical trajectory, suggesting tightly regulated underlying mechanisms (Sigal et al., 2019). Accelerating or delaying the appearances of PNN merely changes the rate of their appearance and not any other structural changes as illustrated by the principal component analysis using several morphological parameters including mean hole size, the contiguity and the mean surface intensity of WFA, the signal contrast, skewness and the uniformity of the WFA signal. This analysis was done on images transformed using Behrmann equal-area cylindrical surface projection that might introduce shape and distance distortions especially at the areas close to sphere "poles". Considering the complex shape of neurons, which are neither spherical nor cylindrical, such estimates can be misleading. We have developed an objective method that accurately measures these parameters in 3D space. We have included in the analysis the shape parameters of PNN units that appeared to be very important parameters to discriminate between treatments.

Another recent study made an excellent effort to quantify the PNN structure using binary gap analysis, analysis of PNN peaks and nodes to calculate the PNN aggregation on the neuronal surface using Z-projected images (Eill et al., 2020). Using local maxima function in Fiji, the authors identified the nodes and used an ad hoc algorithm to measure the average distance between those nodes and quantified the difference in the intensity between the nodes and their surrounding space on the cell surface. Though this method can reliably measure the PNN aggregates on the neuronal surface, it does not provide the 3D information and the fundamental parameters of circular-like perisynaptic ECM units such as the hole area, its perimeter, circularity, etc.

PNNs are composed of CSPGs (especially of aggrecan together with varying degrees of other CSPGs such as brevican, neurocan, phosphocan, versican) assembled on the backbone of hyaluronic acid, stabilized by link proteins and glycoprotein tenascin-R (Morawski, Dityatev, et al., 2014). However, how these variations in the composition of PNN are affecting the fine structure and function of PNNs has not been systematically studied. Additionally, maturation of PNNs involves not only an increased assembly of CSPGs but also changes in the sugar chains (CS-GAGs) attached to the core proteins of CSPGs, which can be further sulfated at the 4 or 6 positions or di-sulfated (Lin, Rosahl, Whiting, Fawcett, & Kwok, 2011). The sulfation of these sugars makes them charged and seems to contribute to their binding to Ca^{2+} ions and larger molecules such as neurotrophins, semaphorin 3A, and the transcription factor Otx2. The changes in the sulfation seem to affect the maturation of PNNs. Increasing the 6-sulfation with overexpression of Chst3 delays the PNN formation while an increase in the 4-sulfation seems to accelerate the PNN formation via Otx2-dependent maturation of PV+ cells. However, how the changes in sulfation structurally contribute to the properties of individual PNN units remains to be an interesting area of research.

Several genetic studies have shown that ECM related genes are associated with mental disorders. One of these is the PNN protein neurocan (Muhleisen et al., 2012; Oruc, Kapur-Pojskic, Ramic, Pojskic, & Bajrovic, 2012; Ripke et al., 2013). Additionally, single nucleotide polymorphism (SNP) of b −1,3-glucuronyltransferase 2, HNK-1 biosynthesis enzyme was reported as a schizophrenia risk allele, correlated with decreased cortex volume in schizophrenic patients (Kahler et al., 2011). Moreover, matrix metalloprotease MMP-16, neuroglycan C, and link protein HAPLN4 were identified as genes associated with this disease. Furthermore, SNP in the HAPLN4 gene lies within the most enriched cis-regulatory elements categories and its gene expression level is associated with multiple SNPs within both promoter and enhancer sequences (Roussos et al., 2014). In addition, 50% reduction of mRNA and protein levels of the ECM glycoprotein reelin responsible for cell–cell interaction in cell migration and orientation process was found in several brain areas, including PFC and hippocampus, in schizophrenia patients (Fatemi et al., 1999; Guidotti et al., 2000; Impagnatiello et al., 1998). Fine structure analysis of PNNs in the appropriate mouse mutants could be instrumental to elucidate the impact of these ECM molecules on the synaptic organization in different brain regions. It would also be very interesting to relate the outcome of these studies with analysis of PNN units under diverse pathological conditions such as schizophrenia, depression, Alzheimer's disease, and epilepsy to understand general and disease-specific PNN abnormalities. One limitation of our novel tool is the lack of measuring the parameters related to the synaptic boutons and correlating them with the parameters of respective

PNN units, that will certainly be addressed in the future modifications of the tool. Moreover, it would be also fascinating to image the dynamic structural changes within individual holes during synaptic plasticity using live imaging methods to elucidate the coordination of ECM, pre- and postsynaptic remodeling processes.

ACKNOWLEDGMENTS

We thank Katrin Boehm for technical support.

CONFLICT OF INTEREST

The authors declare that the research was conducted in the absence of any commercial or financial relationships that could be construed as a potential conflict of interest.

AUTHOR'S CONTRIBUTIONS

A.D. designed the research study and the algorithm of PNN unit analysis. A.B. provided brain samples. G.M. performed immunohistochemical labeling and confocal imaging. N.L. wrote the initial Fiji script, which was further modified by A.D. and R.K.. R.K. analyzed the data using the script. A.K., A.Dv., and M.P. performed the manual analysis of PNN units. A.D. and M.P. performed the statistical analysis. R.K. wrote the initial draft of the manuscript. A.D., G.M. and M.P. edited the manuscript. All authors read and approved the final manuscript.

DATA AVAILABILITY STATEMENT

The data that support the findings of this study are openly available on https://data.mendeley.com/datasets/cvf924fz3p/draft?a=d1d290a3-b039-4fc7-b9de-63090fd4a063. The Fiji script is available upon request to the corresponding author.

ORCID

Rahul Kaushik https://orcid.org/0000-0002-4944-8549
Gabriela Matuszko https://orcid.org/0000-0002-2130-5175
Axel Becker https://orcid.org/0000-0002-3406-3558
Mikhail Paveliev https://orcid.org/0000-0002-2905-2272
Alexander Dityatev https://orcid.org/0000-0002-0472-0553

REFERENCES

Abi-Dargham, A., & Moore, H. (2003). Prefrontal DA transmission at D1 receptors and the pathology of schizophrenia. *Neuroscientist*, *9*, 404–416. https://doi.org/10.1177/1073858403252674

Alcaide, J., Guirado, R., Crespo, C., Blasco-Ibanez, J. M., Varea, E., Sanjuan, J., & Nacher, J. (2019). Alterations of perineuronal nets in the dorsolateral prefrontal cortex of neuropsychiatric patients. *International Journal of Bipolar Disorders*, *7*, 24. https://doi.org/10.1186/s40345-019-0161-0

Arnst, N., Kuznetsova, S., Lipachev, N., Shaikhutdinov, N., Melnikova, A., Mavlikeev, M., … Paveliev, M. (2016). Spatial patterns and cell surface clusters in perineuronal nets. *Brain Research*, *1648*, 214–223. https://doi.org/10.1016/j.brainres.2016.07.020

Banerjee, S. P., Zuck, L. G., Yablonsky-Alter, E., & Lidsky, T. I. (1995). Glutamate agonist activity: Implications for antipsychotic drug action and schizophrenia. *NeuroReport*, *6*, 2500–2504. https://doi.org/10.1097/00001756-199512150-00014

Beasley, C. L., & Reynolds, G. P. (1997). Parvalbumin-immunoreactive neurons are reduced in the prefrontal cortex of schizophrenics. *Schizophrenia Research*, *24*, 349–355. https://doi.org/10.1016/S0920-9964(96)00122-3

Becker, A., Grecksch, G., Zernig, G., Ladstaetter, E., Hiemke, C., & Schmitt, U. (2009). Haloperidol and risperidone have specific effects on altered pain sensitivity in the ketamine model of schizophrenia. *Psychopharmacology (Berl)*, *202*, 579–587. https://doi.org/10.1007/s00213-008-1336-z

Begum, M. R., & Sng, J. C. G. (2017). Molecular mechanisms of experience-dependent maturation in cortical GABAergic inhibition. *Journal of Neurochemistry*, *142*, 649–661. https://doi.org/10.1111/jnc.14103

Berezin, V., Walmod, P. S., Filippov, M., & Dityatev, A. (2014). Targeting of ECM molecules and their metabolizing enzymes and receptors for the treatment of CNS diseases. *Progress in Brain Research*, *214*, 353–388.

Bernard, C., & Prochiantz, A. (2016). Otx2-PNN interaction to regulate cortical plasticity. *Neural Plasticity*, *2016*, 7931693. https://doi.org/10.1155/2016/7931693

Bitanihirwe, B. K., Mauney, S. A., & Woo, T. U. (2016). Weaving a net of neurobiological mechanisms in schizophrenia and unraveling the underlying pathophysiology. *Biological Psychiatry*, *80*, 589–598. https://doi.org/10.1016/j.biopsych.2016.03.1047

Bitanihirwe, B. K., & Woo, T. U. (2014a). Transcriptional dysregulation of gamma-aminobutyric acid transporter in parvalbumin-containing inhibitory neurons in the prefrontal cortex in schizophrenia. *Psychiatry Research*, *220*, 1155–1159.

Bitanihirwe, B. K. Y., & Woo, T. U. W. (2014b). Perineuronal nets and schizophrenia: The importance of neuronal coatings. *Neuroscience & Biobehavioral Reviews*, *45*, 85–99. https://doi.org/10.1016/j.neubiorev.2014.03.018

Bruckner, G., Kacza, J., & Grosche, J. (2004). Perineuronal nets characterized by vital labelling, confocal and electron microscopy in organotypic slice cultures of rat parietal cortex and hippocampus. *Journal of Molecular Histology*, *35*, 115–122. https://doi.org/10.1023/B:HIJO.0000023374.22298.50

Carceller, H., Guirado, R., & Nacher, J. (2019). Dark exposure affects plasticity-related molecules and interneurons throughout the visual system during adulthood. *Journal of Comparative Neurology*, *528*(8), 1349–1366. https://doi.org/10.1002/cne.24832

Carlsson, A. (1995). Neurocircuitries and neurotransmitter interactions in schizophrenia. *International Clinical Psychopharmacology*, *10*(Suppl 3), 21–28.

Carulli, D., Pizzorusso, T., Kwok, J. C., Putignano, E., Poli, A., Forostyak, S., … Fawcett, J. W. (2010). Animals lacking link protein have attenuated perineuronal nets and persistent plasticity. *Brain*, *133*, 2331–2347. https://doi.org/10.1093/brain/awq145

Castillo-Gomez, E., Perez-Rando, M., Vidueira, S., & Nacher, J. (2016). Polysialic acid acute depletion induces structural plasticity in interneurons and impairs the excitation/inhibition balance in medial prefrontal cortex organotypic cultures. *Frontiers in Cellular Neuroscience*, *10*, 170. https://doi.org/10.3389/fncel.2016.00170

Castillo-Gomez, E., Varea, E., Blasco-Ibanez, J. M., Crespo, C., & Nacher, J. (2016). Effects of chronic dopamine D2R agonist treatment and polysialic acid depletion on dendritic spine density and excitatory neurotransmission in the mPFC of adult rats. *Neural Plasticity*, *2016*, 1615363. https://doi.org/10.1155/2016/1615363

Celio, M. R., Spreafico, R., De Biasi, S., & Vitellaro-Zuccarello, L. (1998). Perineuronal nets: Past and present. *Trends in Neurosciences*, *21*, 510–515. https://doi.org/10.1016/S0166-2236(98)01298-3

Chung, D. W., Fish, K. N., & Lewis, D. A. (2016). Pathological basis for deficient excitatory drive to cortical parvalbumin interneurons in schizophrenia. *The American Journal of Psychiatry*, *173*, 1131–1139. https://doi.org/10.1176/appi.ajp.2016.16010025

Dityatev, A., Bruckner, G., Dityateva, G., Grosche, J., Kleene, R., & Schachner, M. (2007). Activity-dependent formation and functions of chondroitin sulfate-rich extracellular matrix of perineuronal nets. *Developmental Neurobiology*, *67*, 570–588. https://doi.org/10.1002/dneu.20361

Dityatev, A., & Fellin, T. (2008). Extracellular matrix in plasticity and epileptogenesis. *Neuron Glia Biology*, *4*, 235–247. https://doi.org/10.1017/S1740925X09000118

Dityatev, A., Frischknecht, R., & Seidenbecher, C. I. (2006). Extracellular matrix and synaptic functions. *Results and Problems in Cell Differentiation*, *43*, 69–97.

Dityatev, A., & Schachner, M. (2003). Extracellular matrix molecules and synaptic plasticity. *Nature Reviews Neuroscience*, *4*, 456–468. https://doi.org/10.1038/nrn1115

Dityatev, A., Schachner, M., & Sonderegger, P. (2010). The dual role of the extracellular matrix in synaptic plasticity and homeostasis. *Nature Reviews Neuroscience*, *11*, 735–746. https://doi.org/10.1038/nrn2898

Dityatev, A., Wehrle-Haller, B., & Pitkanen, A. (2014). Preface. Brain extracellular matrix in health and disease. *Progress in Brain Research*, *214*, xiii–xvii.

Eill, G. J., Sinha, A., Morawski, M., Viapiano, M. S., & Matthews, R. T. (2020). The protein tyrosine phosphatase RPTPzeta/phosphacan is critical for perineuronal net structure. *Journal of Biological Chemistry*, *295*, 955–968.

Enwright, J. F., Sanapala, S., Foglio, A., Berry, R., Fish, K. N., & Lewis, D. A. (2016). Reduced labeling of parvalbumin neurons and perineuronal nets in the dorsolateral prefrontal cortex of subjects with schizophrenia. *Neuropsychopharmacology*, *41*, 2206–2214. https://doi.org/10.1038/npp.2016.24

Fatemi, S. H., Emamian, E. S., Kist, D., Sidwell, R. W., Nakajima, K., Akhter, P., … Bailey, K. (1999). Defective corticogenesis and reduction in Reelin immunoreactivity in cortex and hippocampus of prenatally infected neonatal mice. *Molecular Psychiatry*, *4*, 145–154. https://doi.org/10.1038/sj.mp.4000520

Favuzzi, E., Marques-Smith, A., Deogracias, R., Winterflood, C. M., Sanchez-Aguilera, A., Mantoan, L., … Rico, B. (2017). Activity-dependent gating of parvalbumin interneuron function by the perineuronal net protein brevican. *Neuron*, *95*, 639–655.e10. https://doi.org/10.1016/j.neuron.2017.06.028

Ferrer-Ferrer, M., & Dityatev, A. (2018). Shaping synapses by the neural extracellular matrix. *Frontiers in Neuroanatomy*, *12*, 40. https://doi.org/10.3389/fnana.2018.00040

Frohlich, J., & Van Horn, J. D. (2014). Reviewing the ketamine model for schizophrenia. *Journal of Psychopharmacology*, *28*, 287–302. https://doi.org/10.1177/0269881113512909

Geissler, M., Gottschling, C., Aguado, A., Rauch, U., Wetzel, C. H., Hatt, H., & Faissner, A. (2013). Primary hippocampal neurons, which lack four crucial extracellular matrix molecules, display abnormalities of synaptic structure and function and severe deficits in perineuronal net formation. *Journal of Neuroscience*, *33*, 7742–7755. https://doi.org/10.1523/JNEUROSCI.3275-12.2013

Gomes, F. V., & Grace, A. A. (2018). Cortical dopamine dysregulation in schizophrenia and its link to stress. *Brain*, *141*, 1897–1899. https://doi.org/10.1093/brain/awy156

Grace, A. A. (2016). Dysregulation of the dopamine system in the pathophysiology of schizophrenia and depression. *Nature Reviews Neuroscience*, *17*, 524–532. https://doi.org/10.1038/nrn.2016.57

Guidotti, A., Auta, J., Davis, J. M., Di-Giorgi-Gerevini, V., Dwivedi, Y., Grayson, D. R., … Costa, E. (2000). Decrease in reelin and glutamic acid decarboxylase67 (GAD67) expression in schizophrenia and bipolar disorder: A postmortem brain study. *Archives of General Psychiatry*, *57*, 1061–1069. https://doi.org/10.1001/archpsyc.57.11.1061

Hashimoto, T., Volk, D. W., Eggan, S. M., Mirnics, K., Pierri, J. N., Sun, Z., … Lewis, D. A. (2003). Gene expression deficits in a subclass of GABA neurons in the prefrontal cortex of subjects with schizophrenia. *The Journal of Neuroscience: The Official Journal of the Society for Neuroscience*, *23*, 6315–6326. https://doi.org/10.1523/JNEUROSCI.23-15-06315.2003

Hayani, H., Song, I., & Dityatev, A. (2018). Increased excitability and reduced excitatory synaptic input into fast-spiking CA2 interneurons after enzymatic attenuation of extracellular matrix. *Frontiers in Cellular Neuroscience*, *12*, 149. https://doi.org/10.3389/fncel.2018.00149

Heine, M., Groc, L., Frischknecht, R., Beique, J. C., Lounis, B., Rumbaugh, G., … Choquet, D. (2008). Surface mobility of postsynaptic AMPARs tunes synaptic transmission. *Science*, *320*, 201–205. https://doi.org/10.1126/science.1152089

Heresco-Levy, U. (2005). Glutamatergic neurotransmission modulators as emerging new drugs for schizophrenia. *Expert Opinion on Emerging Drugs*, *10*, 827–844. https://doi.org/10.1517/14728214.10.4.827

Hunt, M. J., Kessal, K., & Garcia, R. (2005). Ketamine induces dopamine-dependent depression of evoked hippocampal activity in the nucleus accumbens in freely moving rats. *Journal of Neuroscience*, *25*, 524–531. https://doi.org/10.1523/JNEUROSCI.3800-04.2005

Impagnatiello, F., Guidotti, A. R., Pesold, C., Dwivedi, Y., Caruncho, H., Pisu, M. G., … Costa, E. (1998). A decrease of reelin expression as a putative vulnerability factor in schizophrenia. *Proceedings of the National Academy of Sciences United States of America*, *95*, 15718–15723. https://doi.org/10.1073/pnas.95.26.15718

Jeevakumar, V., Driskill, C., Paine, A., Sobhanian, M., Vakil, H., Morris, B., … Kroener, S. (2015). Ketamine administration during the second postnatal week induces enduring schizophrenia-like behavioral symptoms and reduces parvalbumin expression in the medial prefrontal cortex of adult mice. *Behavioral Brain Research*, *282*, 165–175. https://doi.org/10.1016/j.bbr.2015.01.010

Kaar, S. J., Angelescu, I., Marques, T. R., & Howes, O. D. (2019). Prefrontal parvalbumin interneurons in schizophrenia: A meta-analysis of post-mortem studies. *Journal of Neural Transmission (Vienna)*, *126*, 1637–1651. https://doi.org/10.1007/s00702-019-02080-2

Kahler, A. K., Djurovic, S., Rimol, L. M., Brown, A. A., Athanasiu, L., Jonsson, E. G., … Andreassen, O. A. (2011). Candidate gene analysis of the human natural killer-1 carbohydrate pathway and perineuronal nets in schizophrenia: B3GAT2 is associated with disease risk and cortical surface area. *Biological Psychiatry*, *69*, 90–96. https://doi.org/10.1016/j.biopsych.2010.07.035

Kapur, S., & Seeman, P. (2002). NMDA receptor antagonists ketamine and PCP have direct effects on the dopamine D(2) and serotonin 5-HT(2)receptors-implications for models of schizophrenia. *Molecular Psychiatry*, *7*, 837–844. https://doi.org/10.1038/sj.mp.4001093

Kaushik, R., Morkovin, E., Schneeberg, J., Confettura, A. D., Kreutz, M. R., Senkov, O., & Dityatev, A. (2018). Traditional Japanese Herbal Medicine Yokukansan Targets Distinct but Overlapping Mechanisms in Aged Mice and in the 5xFAD Mouse Model of Alzheimer's Disease. *Frontiers in Aging Neuroscience*, *10*, 411. https://doi.org/10.3389/fnagi.2018.00411

Kochlamazashvili, G., Henneberger, C., Bukalo, O., Dvoretskova, E., Senkov, O., Lievens, P. M., … Dityatev, A. (2010). The extracellular matrix molecule hyaluronic acid regulates hippocampal synaptic plasticity by modulating postsynaptic L-type Ca(2+) channels. *Neuron*, *67*, 116–128. https://doi.org/10.1016/j.neuron.2010.05.030

Kwok, J. C., Dick, G., Wang, D., & Fawcett, J. W. (2011). Extracellular matrix and perineuronal nets in CNS repair. *Developmental Neurobiology*, *71*, 1073–1089.

Lander, C., Zhang, H., & Hockfield, S. (1998). Neurons produce a neuronal cell surface-associated chondroitin sulfate proteoglycan. *Journal of Neuroscience*, *18*, 174–183. https://doi.org/10.1523/JNEUROSCI.18-01-00174.1998

Lau, C. I., Wang, H. C., Hsu, J. L., & Liu, M. E. (2013). Does the dopamine hypothesis explain schizophrenia? *Reviews in the Neurosciences*, *24*, 389–400. https://doi.org/10.1515/revneuro-2013-0011

Le Gall, E., & Iakimova, G. (2018). Social cognition in schizophrenia and autism spectrum disorder: Points of convergence and functional differences. *Encephale*, *44*, 523–537.

Lin, R., Rosahl, T. W., Whiting, P. J., Fawcett, J. W., & Kwok, J. C. (2011). 6-Sulphated chondroitins have a positive influence on axonal regeneration. *PLoS One*, *6*, e21499. https://doi.org/10.1371/journal.pone.0021499

Lipachev, N., Arnst, N., Melnikova, A., Jaalinoja, H., Kochneva, A., Zhigalov, A., … Paveliev, M. (2019). Quantitative changes in perineuronal nets in development and posttraumatic condition. *Journal of Molecular Histology*, *50*, 203–216. https://doi.org/10.1007/s10735-019-09818-y

Lodge, D. J., Behrens, M. M., & Grace, A. A. (2009). A loss of parvalbumin-containing interneurons is associated with diminished oscillatory activity in an animal model of schizophrenia. *Journal of Neuroscience*, *29*, 2344–2354. https://doi.org/10.1523/JNEUROSCI.5419-08.2009

MacKenzie, L. E., Patterson, V. C., Zwicker, A., Drobinin, V., Fisher, H. L., Abidi, S., … Uher, R. (2017). Hot and cold executive functions in youth with psychotic symptoms. *Psychological Medicine*, *47*, 2844–2853. https://doi.org/10.1017/S0033291717001374

Matuszko, G., Curreli, S., Kaushik, R., Becker, A., & Dityatev, A. (2017). Extracellular matrix alterations in the ketamine model of schizophrenia. *Neuroscience*, *350*, 13–22. https://doi.org/10.1016/j.neuroscience.2017.03.010

McNally, J. M., McCarley, R. W., & Brown, R. E. (2013). Impaired GABAergic neurotransmission in schizophrenia underlies impairments in cortical gamma band oscillations. *Current Psychiatry Reports*, *15*, 346. https://doi.org/10.1007/s11920-012-0346-z

McRae, P. A., Rocco, M. M., Kelly, G., Brumberg, J. C., & Matthews, R. T. (2007). Sensory deprivation alters aggrecan and perineuronal net expression in the mouse barrel cortex. *Journal of Neuroscience*, *27*, 5405–5413. https://doi.org/10.1523/JNEUROSCI.5425-06.2007

Mitelman, S. A., Buchsbaum, M. S., Christian, B. T., Merrill, B. M., Buchsbaum, B. R., Mukherjee, J., & Lehrer, D. S. (2019). Positive association between cerebral grey matter metabolism and dopamine D2/D3 receptor availability in healthy and schizophrenia subjects: An (18)F-fluorodeoxyglucose and (18)F-fallypride positron emission tomography study. *World J Biol Psychiatry*, *20*, 1–15.

Miyata, S., & Kitagawa, H. (2015). Mechanisms for modulation of neural plasticity and axon regeneration by chondroitin sulphate. *Journal of Biochemistry*, *157*, 13–22. https://doi.org/10.1093/jb/mvu067

Miyata, S., Komatsu, Y., Yoshimura, Y., Taya, C., & Kitagawa, H. (2012). Persistent cortical plasticity by upregulation of chondroitin 6-sulfation. *Nature Neuroscience*, *15*, 414–422, S411-412. https://doi.org/10.1038/nn.3023

Moghaddam, B., & Javitt, D. (2012). From revolution to evolution: The glutamate hypothesis of schizophrenia and its implication for treatment. *Neuropsychopharmacology*, *37*, 4–15. https://doi.org/10.1038/npp.2011.181

Morawski, M., Bruckner, M. K., Riederer, P., Bruckner, G., & Arendt, T. (2004). Perineuronal nets potentially protect against oxidative stress. *Experimental Neurology*, *188*, 309–315. https://doi.org/10.1016/j.expneurol.2004.04.017

Morawski, M., Dityatev, A., Hartlage-Rubsamen, M., Blosa, M., Holzer, M., Flach, K., … Schachner, M. (2014). Tenascin-R promotes assembly of the extracellular matrix of perineuronal nets via clustering of aggrecan. *Philosophical Transactions of the Royal Society of London. Series B, Biological Sciences*, *369*, 20140046. https://doi.org/10.1098/rstb.2014.0046

Morawski, M., Filippov, M., Tzinia, A., Tsilibary, E., & Vargova, L. (2014). ECM in brain aging and dementia. *Progress in Brain Research*, *214*, 207–227.

Morris, B. J., Cochran, S. M., & Pratt, J. A. (2005). PCP: From pharmacology to modelling schizophrenia. *Current Opinion in Pharmacology*, *5*, 101–106. https://doi.org/10.1016/j.coph.2004.08.008

Mueser, K. T., & McGurk, S. R. (2004). Schizophrenia. *Lancet (London, England)*, *363*, 2063–2072. https://doi.org/10.1016/S0140-6736(04)16458-1

Muhleisen, T. W., Mattheisen, M., Strohmaier, J., Degenhardt, F., Priebe, L., Schultz, C. C., … Cichon, S. (2012). Association between schizophrenia and common variation in neurocan (NCAN), a genetic risk factor for bipolar disorder. *Schizophrenia Research*, *138*, 69–73. https://doi.org/10.1016/j.schres.2012.03.007

Olney, J. W., & Farber, N. B. (1995). Glutamate receptor dysfunction and schizophrenia. *Archives of General Psychiatry*, *52*, 998–1007. https://doi.org/10.1001/archpsyc.1995.03950240016004

Oruc, L., Kapur-Pojskic, L., Ramic, J., Pojskic, N., & Bajrovic, K. (2012). Assessment of relatedness between neurocan gene as bipolar disorder susceptibility locus and schizophrenia. *Bosnian Journal of Basic Medical Sciences*, *12*, 245–248. https://doi.org/10.17305/bjbms.2012.2446

Patz, S., Grabert, J., Gorba, T., Wirth, M. J., & Wahle, P. (2004). Parvalbumin expression in visual cortical interneurons depends on neuronal activity and TrkB ligands during an Early period of postnatal development. *Cerebral Cortex*, *14*, 342–351. https://doi.org/10.1093/cercor/bhg132

Pizzorusso, T., Medini, P., Berardi, N., Chierzi, S., Fawcett, J. W., & Maffei, L. (2002). Reactivation of ocular dominance plasticity in the adult visual cortex. *Science*, *298*, 1248–1251. https://doi.org/10.1126/science.1072699

Racz, E., Gaal, B., & Matesz, C. (2016). Heterogeneous expression of extracellular matrix molecules in the red nucleus of the rat.

Neuroscience, *322*, 1–17. https://doi.org/10.1016/j.neuroscience.2016.02.005

Reynolds, G. P., Beasley, C. L., & Zhang, Z. J. (2002). Understanding the neurotransmitter pathology of schizophrenia: Selective deficits of subtypes of cortical GABAergic neurons. *Journal of Neural Transmission (Vienna)*, *109*, 881–889. https://doi.org/10.1007/s007020200072

Riga, D., Kramvis, I., Koskinen, M. K., van Bokhoven, P., van der Harst, J. E., Heistek, T. S., … Spijker, S. (2017). Hippocampal extracellular matrix alterations contribute to cognitive impairment associated with a chronic depressive-like state in rats. *Science Translational Medicine*, *9*(421), eaai8753. https://doi.org/10.1126/scitranslmed.aai8753

Ripke, S., O'Dushlaine, C., Chambert, K., Moran, J. L., Kahler, A. K., Akterin, S., … Rujescu, D. A. (2013). Genome-wide association analysis identifies 13 new risk loci for schizophrenia. *Nature Genetics*, *45*, 1150–1159. https://doi.org/10.1038/ng.2742

Roussos, P., Mitchell, A. C., Voloudakis, G., Fullard, J. F., Pothula, V. M., Tsang, J., … Sklar, P. (2014). A role for noncoding variation in schizophrenia. *Cell Reports*, *9*, 1417–1429. https://doi.org/10.1016/j.celrep.2014.10.015

Sakai, T., Oshima, A., Nozaki, Y., Ida, I., Haga, C., Akiyama, H., … Mikuni, M. (2008). Changes in density of calcium-binding-protein-immunoreactive GABAergic neurons in prefrontal cortex in schizophrenia and bipolar disorder. *Neuropathology*, *28*, 143–150. https://doi.org/10.1111/j.1440-1789.2007.00867.x

Sigal, Y. M., Bae, H., Bogart, L. J., Hensch, T. K., & Zhuang, X. (2019). Structural maturation of cortical perineuronal nets and their perforating synapses revealed by superresolution imaging. *Proceedings of the National Academy of Sciences United States of America*, *116*, 7071–7076. https://doi.org/10.1073/pnas.1817222116

Slifstein, M., van de Giessen, E., Van Snellenberg, J., Thompson, J. L., Narendran, R., Gil, R., … Abi-Dargham, A. (2015). Deficits in prefrontal cortical and extrastriatal dopamine release in schizophrenia: A positron emission tomographic functional magnetic resonance imaging study. *JAMA Psychiatry*, *72*, 316–324. https://doi.org/10.1001/jamapsychiatry.2014.2414

Sohal, V. S. (2014). Identifying pathways leading to prefrontal GABA-ergic interneuron dysfunction in schizophrenia. *American Journal of Psychiatry*, *171*, 906–909. https://doi.org/10.1176/appi.ajp.2014.14060750

Soleman, S., Filippov, M. A., Dityatev, A., & Fawcett, J. W. (2013). Targeting the neural extracellular matrix in neurological disorders. *Neuroscience*, *253*, 194–213. https://doi.org/10.1016/j.neuroscience.2013.08.050

Sorg, B. A., Berretta, S., Blacktop, J. M., Fawcett, J. W., Kitagawa, H., Kwok, J. C., & Miquel, M. (2016). Casting a Wide Net: Role of Perineuronal Nets in Neural Plasticity. *Journal of Neuroscience*, *36*, 11459–11468. https://doi.org/10.1523/JNEUROSCI.2351-16.2016

Stefanovic, A., Brandner, B., Klaassen, E., Cregg, R., Nagaratnam, M., Bromley, L. M., … Curran, H. V. (2009). Acute and chronic effects of ketamine on semantic priming: Modeling schizophrenia? *Journal of Clinical Psychopharmacology*, *29*, 124–133. https://doi.org/10.1097/JCP.0b013e31819a4b91

Steullet, P., Cabungcal, J. H., Bukhari, S. A., Ardelt, M. I., Pantazopoulos, H., Hamati, F., … Berretta, S. (2018). The thalamic reticular nucleus in schizophrenia and bipolar disorder: Role of parvalbumin-expressing neuron networks and oxidative stress. *Molecular Psychiatry*, *23*, 2057–2065. https://doi.org/10.1038/mp.2017.230

Stone, J. M., Erlandsson, K., Arstad, E., Squassante, L., Teneggi, V., Bressan, R. A., … Pilowsky, L. S. (2008). Relationship between ketamine-induced psychotic symptoms and NMDA receptor occupancy: A [(123)I]CNS-1261 SPET study. *Psychopharmacology (Berl)*, *197*, 401–408. https://doi.org/10.1007/s00213-007-1047-x

Tooney, P. A., & Chahl, L. A. (2004). Neurons expressing calcium-binding proteins in the prefrontal cortex in schizophrenia. *Progress in Neuro-Psychopharmacology & Biological Psychiatry*, *28*, 273–278. https://doi.org/10.1016/j.pnpbp.2003.10.004

Vernaleken, I., Klomp, M., Moeller, O., Raptis, M., Nagels, A., Rosch, F., … Grunder, G. (2013). Vulnerability to psychotogenic effects of ketamine is associated with elevated D2/3-receptor availability. *International Journal of Neuropsychopharmacology*, *16*, 745–754. https://doi.org/10.1017/S1461145712000764

Wang, Y., Chan, R. C. K., & Shum, D. H. K. (2018). Schizophrenia and prospective memory impairments: A review. *The Clinical Neuropsychologist*, *32*, 836–857. https://doi.org/10.1080/13854046.2017.1406144

Woo, T. U., Miller, J. L., & Lewis, D. A. (1997). Schizophrenia and the parvalbumin-containing class of cortical local circuit neurons. *American Journal of Psychiatry*, *154*, 1013–1015.

Yang, N. B., Tian, Q., Fan, Y., Bo, Q. J., Zhang, L., Li, L., & Wang, C. Y. (2017). Deficits of perceived spatial separation induced prepulse inhibition in patients with schizophrenia: Relationships to symptoms and neurocognition. *BMC Psychiatry*, *17*, 135. https://doi.org/10.1186/s12888-017-1276-4

SUPPORTING INFORMATION

Additional supporting information may be found online in the Supporting Information section.

How to cite this article: Kaushik R, Lipachev N, Matuszko G, et al. Fine structure analysis of perineuronal nets in the ketamine model of schizophrenia. *Eur J Neurosci*. 2021;53:3988–4004. https://doi.org/10.1111/ejn.14853